



UNIVERSITY OF PISA
DEPARTMENT OF INFORMATION ENGINEERING

Robotics and Automation Engineering
Master Degree thesis

Human-like motion planning and sensorless control framework for bimanual grasping of cumbersome objects

Supervisor:

Prof: Matteo Bianchi

Ing: Marco Baracca

Ing: Stefano Angeli

Candidate:

Luca Morello

Abstract

In scenarios involving complex object manipulation, certain tasks, such as handling cumbersome objects, require the collaboration of multiple robotic arms acting in a synergistic way. This thesis implements a modular control law within the framework of a multi-manual setup, focusing on tasks involving the picking of unknown objects. Drawing inspiration from force and impedance control principles, a novel adaptation policy is implemented to address inherent limitations observed in conventional methods, including coupled impedance and hybrid position/force control approaches incorporating human-like motion planning and relying on the information from one RGB-D camera only.

The generated point cloud is rigorously filtered and evaluated to account for incomplete surface coverage. This allows significant geometric parameters to be extracted, including the dimensions of the bounding boxes related to the manipulated object and the relative contact point identification. The experimental setup consists of two Franka manipulators. In the initial phase, the system thoroughly assesses the object to find the critical contact areas needed for the manipulation operations that follow. In the contact phase, an impedance control policy is used. In the post-contact phase a hybrid control policy is used to lift and manipulate the object

1 Introduction

Robots are increasingly used in human environments, with industries expecting humanoid robots to replace human workers without redesigning workspaces. In home and healthcare settings, robots must suit human-centric environments. As technology advances, humanoid robots will better mimic human movements and manipulation skills.

Interest in dual-arm manipulation has grown, adding complexity and challenges not present in single-arm systems. Addressing these requires sophisticated integration, planning, reasoning, and control strategies. This complexity drives the development of technologies for coordinating multiple robots' motions [1] [2] [3], controlling motion and force[4], and optimizing contact forces in real-time using techniques like quadratic programming[5][6].

Cooperative multi-arm systems need to control both an object's motion and internal stresses. A force controller can regulate force on the object's surface and estimate external wrenches by comparing applied torque with model-based instructions.

Previous research focused on manipulation assuming contact was already made.

The study explores the impact of imperfect grasp due to vision and approach control inaccuracies on manipulation outcomes. It aims to fill a research gap by proposing a method to identify objects and coordinate manipulator movements using gathered information.

An RGB-D camera provides the workspace's point cloud, allowing the vision node to filter and cluster data to identify potential contact points without prior knowledge of the object. Using this data, a Human-Like trajectory is planned for manipulators to contact the object. In the final stage, hybrid control (combining force and Cartesian control) ensures a stable grip, facilitating subsequent manipulation.

2 Problem formulation

I have been working with a framework consisting of two seven-jointed manipulators that are firmly grasping a common rigid object. In order to satisfy a stable grasp, each manipulator must apply a normal force $^{ee}f_d$ at their contact points. [4] proposes a unified control policy for all manipulators. This algorithm, designed for an n-DoF manipulator, assumes that ^{ee}R rotates its frame with respect to the task frame. The other cooperative arms will use the same algorithm with their associated frame rotation matrix (see Fig. 1). Assuming a stable grasp between the end-effector and the object, we define the end-effector's vector $^{ee}p_{cr}$ within its frame, linking to the object's rotation center. This common point among all manipulators is critical as it gives a uniform reference for all robots. This is necessary in our dual-arm framework for preserving modularity by controlling the object's center of rotation in lieu of individual manipulator control. To relate velocities, I define the Jacobian matrix $J_{cr} \in \mathbb{R}^{6 \times 6}$, with x and x_{ee} representing the Cartesian poses of the object's rotation center and manipulator end-effector, respectively.

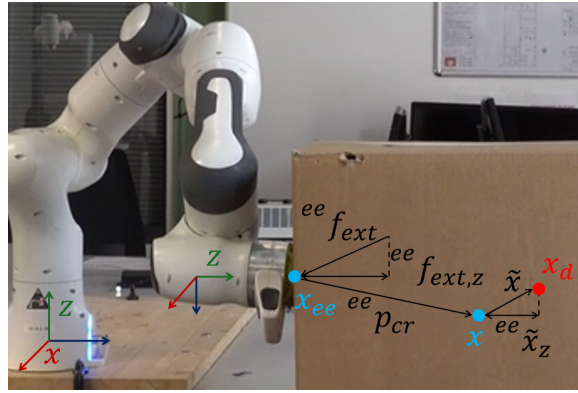


Fig. 1: Each arm has its own set of motion and force variables. The scalars ${}^{ee}f_{ext,z}$ and ${}^{ee}\tilde{x}_z$ represent the projection of the external wrench and the object pose error onto the z-axis of the end-effector frame.

$$\dot{x} = J_{cr}\dot{x}_{ee} \quad J_{cr} = \begin{bmatrix} I_3 & S([{}^{ee}p_{cr}]^T) \\ 0_3 & I_3 \end{bmatrix} \quad (1)$$

As a consequence, the manipulator joint velocities can be mapped into Cartesian space at the object's center of rotation through:

$$\dot{x} = \underbrace{J_{cr}J_{ee}(q)}_{J(q)}\dot{q} \quad (2)$$

At last, the dynamics of the manipulator in Cartesian space can be defined with respect to the object's center of rotation in the following way:

$$M_C(q)\ddot{x} + C_C(q\dot{q})\dot{x} + f_g(q) = f_{in} + J_{cr}^{-T}f_{ext} \quad (3)$$

in which $f_{ext} \in \mathbb{R}^6$ is the external wrench acting on the robot

3 Control design

This Hybrid control framework employ two controllers: one for maintaining grasp and the other for object movement. The conflict between the desired force direction and the trajectory is a major challenge, particularly when the motion opposes the grasping force resulting in a chance of grasp failure or contact loss. These two parts make up the control framework of any present manipulator. The control torque τ_{in} can be expressed as follows:

$$\tau_{in} = \tau_{imp} + \tau_{frc} \quad (4)$$

$\tau_{imp}, \tau_{frc} \in \mathbb{R}^n$ stand for the input torques for motion control and contact force control, respectively.

3.1 Variables Impedance Control

Position control due its high stiffness can result in substantial force buildup. In the literature, one of the most used solution to avoid this problem is the impedance control [7]. This algorithm permits to achieve a compliant behaviour also in rigid kinematic chains, allowing a safe interaction with the environment. This result can be accomplished at the center of rotation of the object by this particular control law.

$$\tau_{imp} = J^T(q)(K_C\tilde{x} + D_C\dot{\tilde{x}} + M_C(q)\ddot{x}_d + C_C(q, \dot{q})\dot{x}_d) \quad \text{with} \quad \tilde{x} = x_d - x$$

In the above formulation, the stiffness and damping matrices are represented by $K_C, D_C \in \mathbb{R}^{6 \times 6}$, and x_d is the desired object pose expressed to the robot frame. The conflict between desired motion and force directions as previously mentioned is a prevalent issue in hybrid force/motion control. To address this, [4] propose an adapting stiffness matrix ${}^{ee}K_C \in \mathbb{R}^{6 \times 6}$ within the robot end-effector frame and continuously transforming it into the robot frame via the rotation matrix ${}^{ee}R^T \in \mathbb{R}^{3 \times 3}$. The following is a description of the adaptive stiffness policy:

$${}^{ee}K_C = \text{diag}([k_{t,x}, k_{t,y}, \rho_{imp}k_{t,z}, k_{r,x}, k_{r,y}, k_{r,z}]) \quad \rho_{imp} = \begin{cases} 1 & \text{If } \delta_{imp} \leq {}^{ee}\tilde{x}_z \\ 0.5(1 - \cos(\pi \frac{{}^{ee}\tilde{x}_z}{\delta_{imp}})) & \text{If } 0 \leq {}^{ee}\tilde{x}_z < \delta_{imp} \\ 0 & \text{Otherwise} \end{cases} \quad (5)$$

The parameters $k_i \in \mathbb{R}^{>0}$ in (5) represent the default stiffness coefficients for translation and rotation, while ${}^{ee}\tilde{x}_z$ define the pose error in the end-effector's z -axis frame. The distance δ_{imp} denotes the starting point of stiffness adaptation along the z -direction of the end-effector. When desired motion conflicts with a secure grasp, this adaptation prioritizes contact forces, hence the overall stability.

3.2 Force control

In case of bimanual non-prehensile manipulation, a precise desired amount of force has to be applied to ensure a firm grasp. However, achieving this result only implementing impedance control is very difficult and makes the whole system not robust to scenario uncertainties (i.e. dimension of the object to be manipulated). Force control strategies typically fall into two categories: direct force control like the one implemented and indirect force control. While direct force control enables direct control of contact forces via a force feedback loop, indirect force control regulates force through motion control without explicitly closing a force feedback loop.

Each manipulator must apply a contact force ${}^{ee}f_d$ along the z -direction of the end-effector frame when performing object-grabbing manipulation tasks. The contact force operating along the z -direction of the end-effector is represented by ${}^{ee}f_{ext,z}$ in the force control law. As an outcome, the following represents the expression of the proposed control law:

$$\tau_{frc} = J_{ee}^T(q) \underbrace{[{}^{ee}R, 0_{3 \times 3}]^T [0, 0, \rho_{frc} {}^{ee}f_{frc}]^T}_{f_{frc}} \quad (6)$$

$${}^{ee}f_{frc} = {}^{ee}f_d + k_p {}^{ee}\tilde{f}_{ext} + k_i \int {}^{ee}\tilde{f}_{ext} dt + k_d {}^{ee}\dot{\tilde{f}}_{ext} \quad (7)$$

$$\tilde{f}_{ext} = {}^{ee}f_d + {}^{ee}f_{ext,z} \quad (8)$$

The force controller output f_{frc} is transformed from the end-effector frame ${}^{ee}f_{frc}$ to the robot frame. The controller's behavior is shaped by the proportional, integral, and derivative gains k_p , k_i , and k_d . When the manipulator deviates significantly from the set-point in the z -direction of the end-effector's frame, a control variable labeled ρ_{frc} as described below disables the force controller, preventing unwanted motion, particularly in contact loss scenarios.

$$\rho_{frc} = \begin{cases} 0 & \text{If } 2\delta_{frc} \leq |{}^{ee}\tilde{x}_z| \\ 0.5(1 + \cos(\pi(\frac{{}^{ee}\tilde{x}_z}{\delta_{frc}} - 1))) & \text{If } \delta_{frc} \leq |{}^{ee}\tilde{x}_z| < 2\delta_{frc} \\ 1 & \text{Otherwise} \end{cases} \quad (9)$$

with $\delta_{frc} \in \mathbb{R}^{>0}$ being the threshold in which the force controller gets disabled.

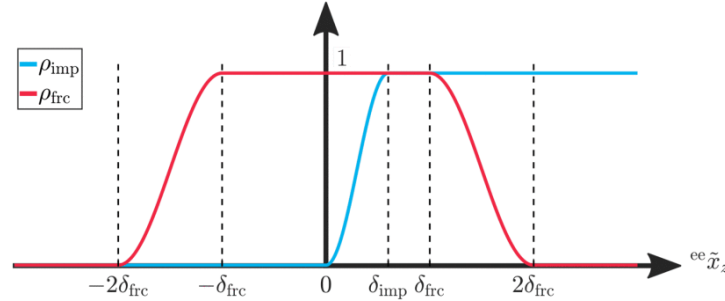


Fig. 2: In this setup, ρ_{frc} activates the force controller only when the positional error along the z -axis within the end-effector frame falls within acceptable threshold. Whereas, ρ_{imp} only triggers the motion controller when the robot is directed to move through the end-effector's z -axis (${}^{ee}\tilde{x}_z > 0$). The end-user defines the parameters δ_{frc} and δ_{imp} in order to evaluate the error ${}^{ee}\tilde{x}_z$ and adjust the related parameters' features.

4 Integrating Orientation to motion planning

I addressed before the issues of selecting an external reference point linked to each manipulator's relative position. However [4], focuses solely on positional data, neglecting orientation considerations thus limiting motion planning only to translational movements.

For rotational manipulation, each manipulator requires different orientations, in [4] can be achieved by directly planned each trajectory, contradicting the modularity principle. In which suggests planning the object's trajectory with robots adapting accordingly. To overcome this, orientation information must be included in the external reference transformations.

During a stable grasp, the displacement between the object and the end-effector remains constant.

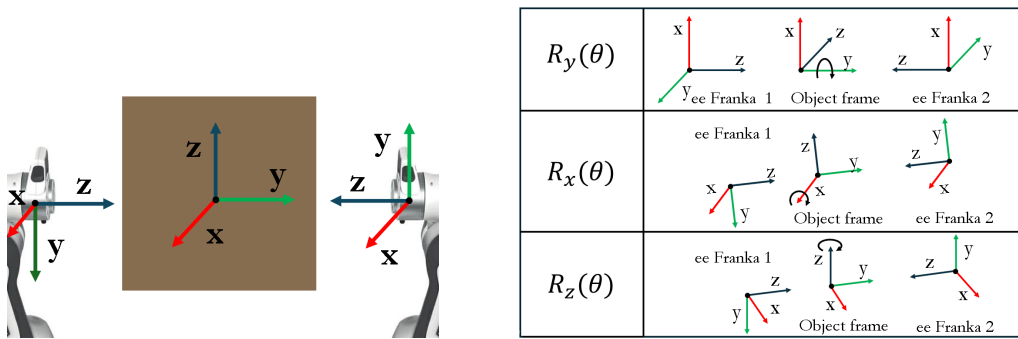


Fig. 3: Object Grasp orientation configuration

The novel theoretical proposed strategy establishes a reference frame instead of a single point to easily identifying the transformations between the end-effectors and the object,(see Fig. 3).

Using then a parameterization such as roll-pitch-yaw on the object, it possible to determine the final configuration the end-effector should assume.

A critical aspect of this framework's design is accounting for additional force components in the desired contact force due to object rotation, particularly from the object's gravitational force. Since the contact forces are estimated, the same approach, introduced in the next section, can be used to identify the weight component acting on the manipulator. An adaptable force design can integrate a corrective term to compensate for the weight's force component.

5 Sensorless Force Estimation

To permit the proposed framework to use force control, the information regarding the force applied by the robot on the grasped object is required. The easiest way to gather this information is to introduce a force/torque sensor at the contact point and directly measure the interaction force. However, reliable force sensors are usually very expensive and fragile, and the complexity of the entire setup would increase dramatically. An interesting solution is the one proposed in [8], where the authors were able to estimate the external torque applied to a manipulator in case of collisions with external obstacles. The monitoring strategy presents a generalized momentum observer outlined in [8], [9], and [10]. It bypasses the requirement of the joint accelerations and the inertia matrix inversion of the robot. This approach seeks to lessen computational burden while improving accuracy and dependability.

$$p = M(q)\dot{q} \quad (10)$$

$$\dot{p} = \tau_{tot} - \tau_F + \dot{M}(q)\dot{q} - C(q, \dot{q})\dot{q} - g(q) \quad \text{with } \dot{M}(q) = C(q, \dot{q}) + C^T(q, \dot{q}) \quad (11)$$

$$= \tau_{tot} - \tau_F + C^T(q, \dot{q})\dot{q} - g(q) \quad (12)$$

The resulting simplified dynamics, derived from the formulation of p , can be roughly summed up as follows:

$$\dot{\hat{p}} = \tau_m + g(q) - \hat{C}^T(q, \dot{q})\dot{q} + r \quad (13)$$

$$\dot{r} = K_O(\dot{p} - \dot{\hat{p}}) \quad (14)$$

$$\dot{r} = K_O(\tau_{ext} - r) \quad (15)$$

$$r = K_O \left(p(t) - \int_0^t \dot{p}(s)ds - p(0) \right) \quad (16)$$

The core equation yields a linearly decoupled stable first-order approximation of the external collision joint torque. The torque estimation dynamics and the monitoring vector r can be easier to comprehend through componentwise analysis in Laplace domain.

$$r_i = \frac{k_{O,i}}{s + k_{O,i}} \tau_{ext,i} = \frac{1}{1 + T_{O,i}s} \tau_{ext,i}, \quad i = 1, \dots, n. \quad (17)$$

Higher values of K_O lead to shorter time constants $T = 1/K_O$ in the transient response, giving the momentum observer properties similar to a virtual joint torque sensor along the robot structure.

However, a major drawback is the fine-tuning needed for the observer gain. While high gain ensures quick response to torque variations, it introduces constant noise, which is especially bothersome in this low-contact force framework. Careful gain adjustment is required to strike a balance among response dynamics and noise interference.

6 Vision and Contact Point identification

Object detection is critical for complete scene understanding in computer vision. Despite significant progress, recognizing objects in cluttered backgrounds remains challenging, particularly for similar-shaped objects. To address this, I propose using image segmentation to identify objects in ambiguous backgrounds. This approach captures a portion of the scene's objects using a point cloud and requires no prior knowledge of objects or 3D models. The goal is to determine the feasible 3D contact points for enabling a stable grasp with both manipulators. Recent research has looked into learning-based approaches to this problem, utilizing RGB-D images to determine optimal grasping rectangles via supervised machine learning. However, these methods require a large amount of data to generalize effectively. Given these challenges, the proposed approach proves to be more adaptable and easier to implement in situations where the shapes can change, making it a viable option in less demanding scenarios.

6.1 Point cloud segmentation

This process seeks to group points with similar features into consistent regions. However, object segmentation in 3D point clouds can be challenging due to noise, sparsity, and data uncertainty. In addition, uneven point distribution and sharp, randomly shaped surfaces make the task more difficult. The limitations of 3D sensors blur background and foreground objects, making it tough to develop accurate identification algorithms. In environments where only one side scan is available, incomplete surface coverage renders the task even more difficult, as illustrated in Fig. 4. Edge detection techniques are unsuitable due to low point density and inaccurate edges. Instead, neighborhood-based methods are recommended. These techniques estimate object dimensions and shape across the point cloud by leveraging the neighbourhood information surrounding each point. This method allows for more comprehensive representations of objects, even in situations with limited surface visibility, by computing regions corresponding to individual objects and accurate reconstructing them with bounding boxes.

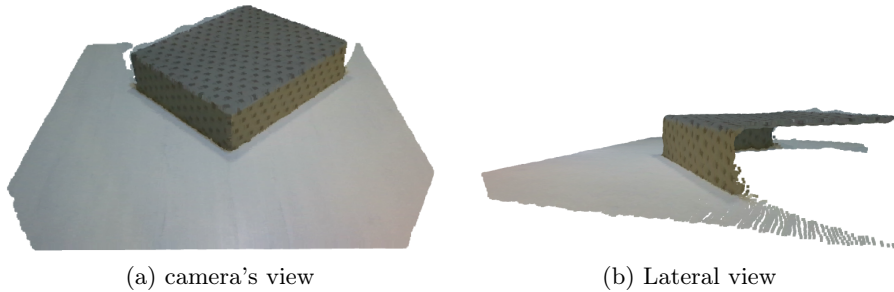


Fig. 4: object segmentation in clear environment

Initial processing [11] is crucial to achieve comprehensive evaluation of point cloud data, which as already mentioned contains noise and distortions. Voxel downsampling is the very first step in the process, which uses Open3D package to reduce data density while keeping crucial features. This stage streamlines the process of outlier removal later on increasing computational efficiency. Subsequently the statistical outlier removal function is applied to eliminate points which significantly differ from their neighbors. This involves determining the average distance between every point and its neighbors, and removing the ones beyond a set threshold. The function needs two parameters as inputs:

- Neighbor Number: Determines how many neighbors are considered when calculating the average distance. A higher value increases robustness against noise but might remove valid points.
- Std Ratio: Sets the threshold level based on the standard deviation of average distances across the point cloud. A lower ratio results in a more aggressive filter.

Fine-tuning these parameters customizes the outlier removal process, resulting in higher data quality for further analysis. This filtering stage is essential for lowering noise, particularly in regions with low point density, such as corners, and improving the precision and accuracy of the contact point. Within this framework, the only practical method for data segmentation is local point cloud clustering. An implementation of DBSCAN [12], a density-based algorithm that works well with asymmetric cluster shapes, is offered by the package Open3D. DBSCAN needs two inputs:

- Eps: The maximum distance between adjacent points within a cluster.
- Min Points: The minimum number of points required to form a cluster.

Following the process of clustering, each cluster's oriented bounding boxes are found, offering a reduced depiction of the cluster's spatial extent. Analysis of contact points is aided by this. The improvements in bounding box accuracy following the application of these filtering techniques to point cloud data segmentation are shown in 5

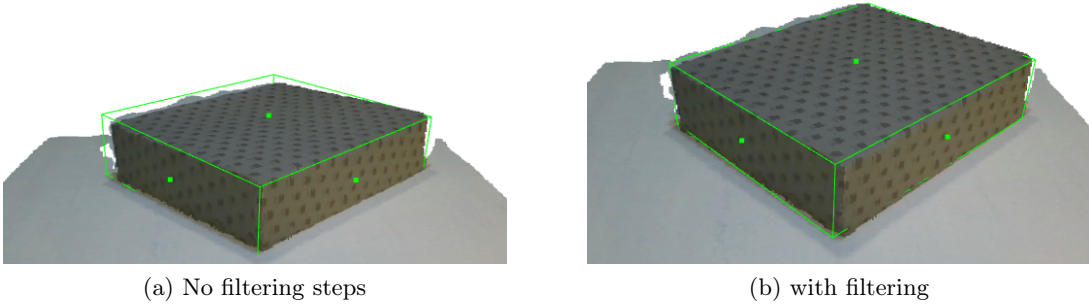


Fig. 5: Oriented Bounding box and contact points analysis

7 Human-Like Motion Planning

One of the features desired for this framework is the ability to generate movements similar to the ones performed by human. The main reason for this choice is that Human-Likeness is a key characteristic for artificial systems designed for a safe, effective and trustworthy human-machine interaction, e.g. with humanoid robots [13, 14]

Among the several algorithms presented in the literature that address the problem of generating human-like motions, I decide to implement the one proposed in [15]. The motivation behind this choice is that the proposed approach shows low computational time and it is already designed in the Cartesian domain, which permits an easier integration with the overall framework.

To summarize, in [15] the authors exploited functional Principal Components Analysis (fPCA) to extract the main characteristics of human upper limb motion and they embed them in a planning algorithm. For the sake of space in the following I report only a brief explanation of the approach while, for more detailed explanation, I refer the interested reader to [16] for the results of fPCA on the Cartesian human hand motion and to [15] for the details of the motion planning algorithm.

7.1 Functional Principal Component Analysis (fPCA)

Functional Principal Component Analysis (fPCA) is a statistical method used to identify the fundamental building blocks of functions, which can then be combined to recreate time series data. The method allows to represent a generic motion of the hand, denoted as $x(t)$, as a combination of weighted basis functions $S_i(t)$, also known as functional Principal Components (fPCs) [17], derived from the dataset.

$$x(t) \approx \bar{x} + S_0(t) + \sum_{i=1}^{s_{max}} \alpha_i \circ S_i(t) \quad (18)$$

In the equation, \bar{x} denotes the average pose of the hand, and $S_0(t)$ the average trajectory observed over all trajectories in the dataset. α_i is a vector of weights, s_{max} is the number of basis elements, and $S_i(t)$ is the i -th basis element. The sign " \circ " represents the Hadamard product, which is element-wise multiplication. The time axis (t) ranges from 0 to 1 representing normalized time.

The first element of the functional basis or first fPC can be computed from the R motions of the dataset as:

$$\max_{S_1} \sum_{j=1}^R \left(\int S_1(t) x_j(t) dt \right)^2 \quad (19)$$

subject to

$$\|S_1(t)\|_2^2 = 1 \quad (20)$$

The other components $S_i(t)$ can be computed as:

$$\max_{S_i} \sum_{j=1}^R \left(\int S_i(t) x_j(t) dt \right)^2 \quad (21)$$

subject to

$$\|S_i(t)\|_2^2 = 1 \quad (22)$$

$$\int_0^{t_{end}} S_i(t) S_k(t) dt = 0, \forall k \in \{1, \dots, i-1\} \quad (23)$$

In this manner, I can identify a basis of functional elements, ordered in terms of the explained variance that each element accounts for.

In [15], the authors applied this analysis to a dataset containing the upper limb movements of 30 different activities of daily living [18]. They found that this reduced functional representation is able to explain up to 90% of the total variance of the dataset with the first 5 fPCs. A more detailed discussion on these results can be found in [16].

7.2 Planning algorithm

The fPCs extracted from a dataset representing common upper limb movements can be used to plan trajectories with intrinsic human-like characteristics. Of note, fPCA is performed for each Degree of Freedom (DoF) separately that, in my case, are the Cartesian position and orientation of the end-effector. In the following, I report the equations for a single DoF of the end effector, while the extension to multiple DoFs (e.g. the six DoFs describing the pose of the end effector) is trivial.

To find the coefficients \bar{x} and α_i given a set of constraints to be satisfied I can define, starting from (18), an equation system to obtain the desired trajectory to be planned. For example, setting the initial and final position, velocity and acceleration, the following equation system is defined:

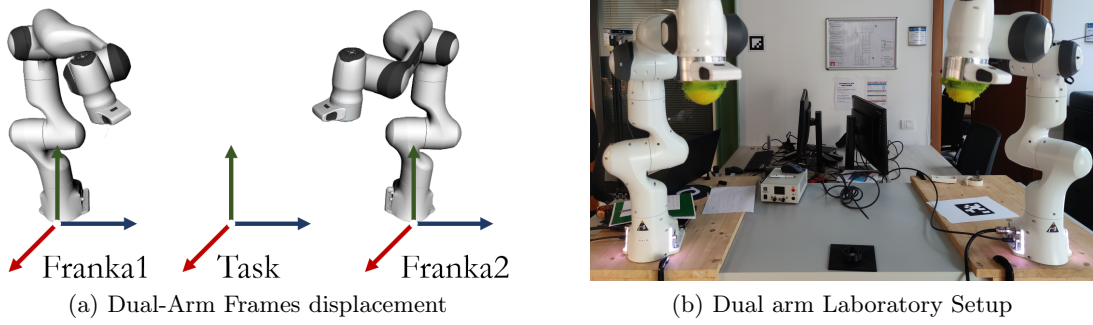
$$\begin{bmatrix} 1 & S_1(t_0) & \dots & S_5(t_0) \\ 1 & S_1(t_f) & \dots & S_5(t_f) \\ 0 & \dot{S}_1(t_0) & \dots & \dot{S}_5(t_0) \\ 0 & \dot{S}_1(t_f) & \dots & \dot{S}_5(t_f) \\ 0 & \ddot{S}_1(t_0) & \dots & \ddot{S}_5(t_0) \\ 0 & \ddot{S}_1(t_f) & \dots & \ddot{S}_5(t_f) \end{bmatrix} \begin{bmatrix} \bar{x} \\ \alpha_1 \\ \alpha_2 \\ \alpha_3 \\ \alpha_4 \\ \alpha_5 \end{bmatrix} = \begin{bmatrix} x(t_0) - S_0(t_0) \\ x(t_f) - S_0(t_f) \\ \dot{x}(t_0) - \dot{S}_0(t_0) \\ \dot{x}(t_f) - \dot{S}_0(t_f) \\ \ddot{x}(t_0) - \ddot{S}_0(t_0) \\ \ddot{x}(t_f) - \ddot{S}_0(t_f) \end{bmatrix} \quad (24)$$

With the obtained weights, the desired trajectory can be computed by exploiting the weighted sum defined in the fPCA formulation to compute the desired motion:

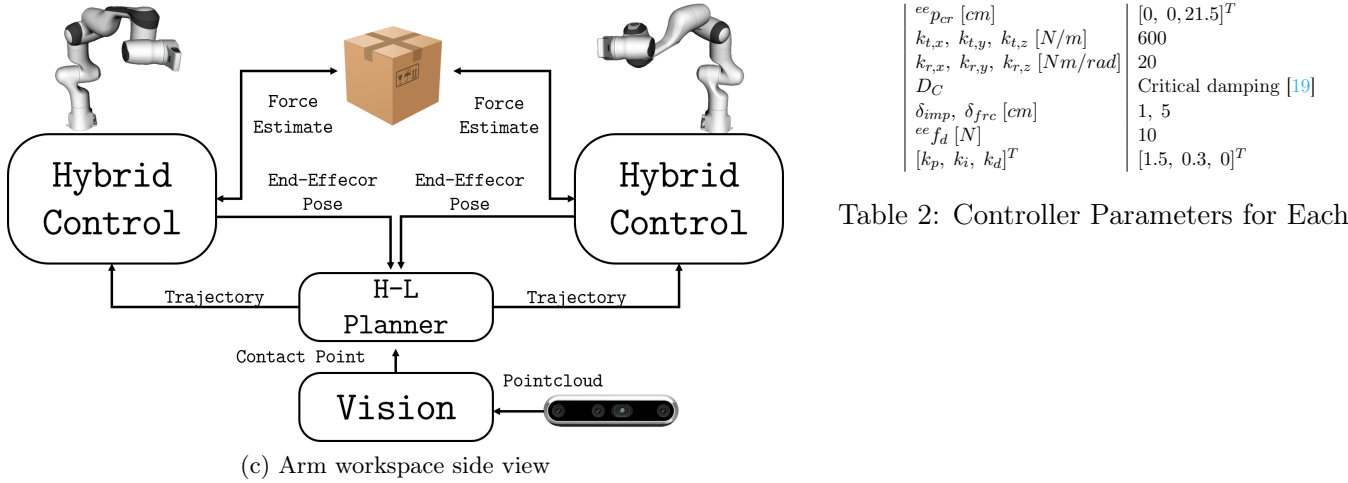
$$x(t) = \bar{x} + S_0(t) + \sum_{i=1}^5 \alpha_i S_i(t) \quad (25)$$

8 Experimental Setup

The experimental setup includes of two Franka manipulators positioned with a displacement of $1.3m$ along the local frames' y -axis, while sharing the same local orientation, specification of the manipulators can be found in [xx]. In order to optimize workflow, a virtual reference system, already referred to as the "Task frame," is utilized. It is located exactly halfway between the two manipulators. This extra frame will be used to define the specific positional coordinates for each robot, while maintaining the same orientation as the local frames of the manipulators.



This approach enables efficient manipulation planning by using the Task frame as the only point of reference. The following section details the experiments that were carried out in order to evaluate the efficiency and stability of control when manipulating objects that would be impossible for a single robotic arm to handle. The item in question is a package with measurements are the following, 40.5 cm height, 42 cm width, 31 cm depth, 0.780 Kg weight.



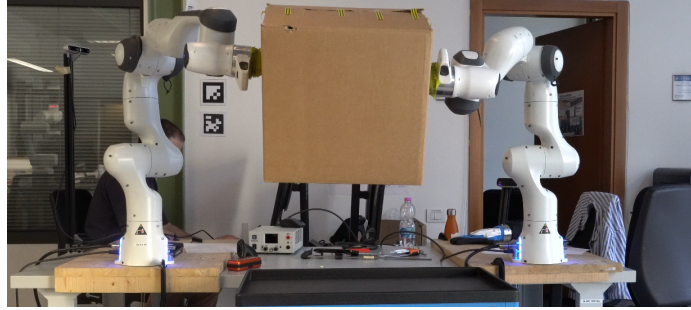
8.1 Pick-up Task



(a) Starting from a generic configuration



(b) Switching to hybrid control policy after the contact point reaching

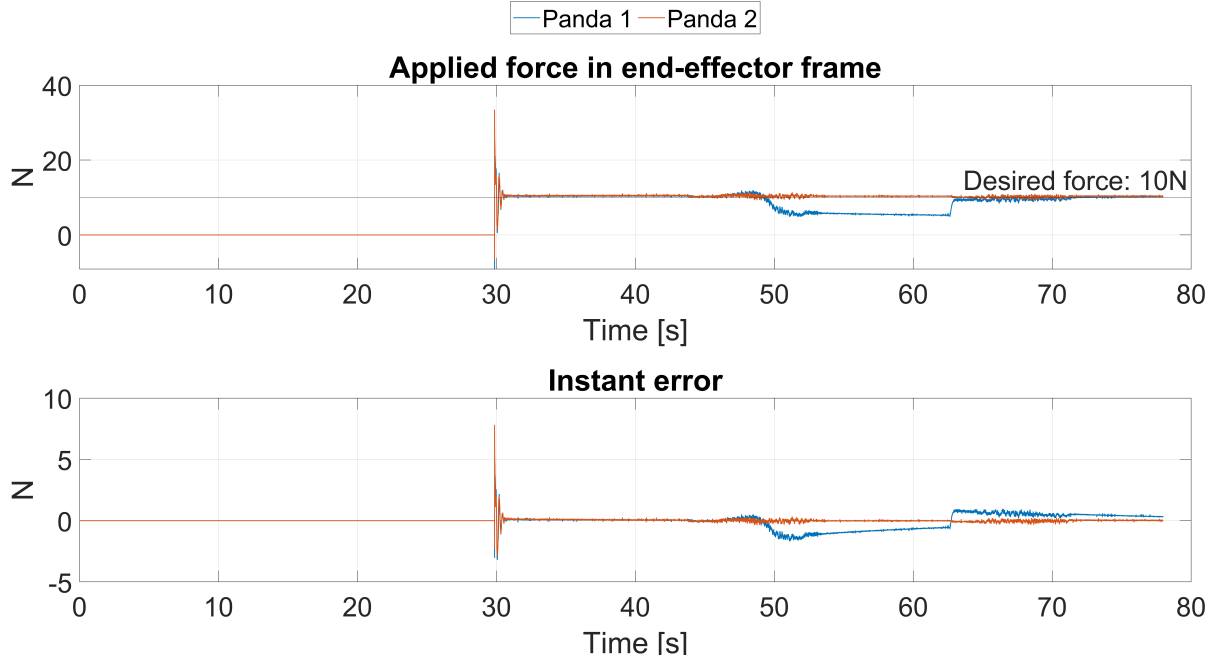


(c) object's pick-up

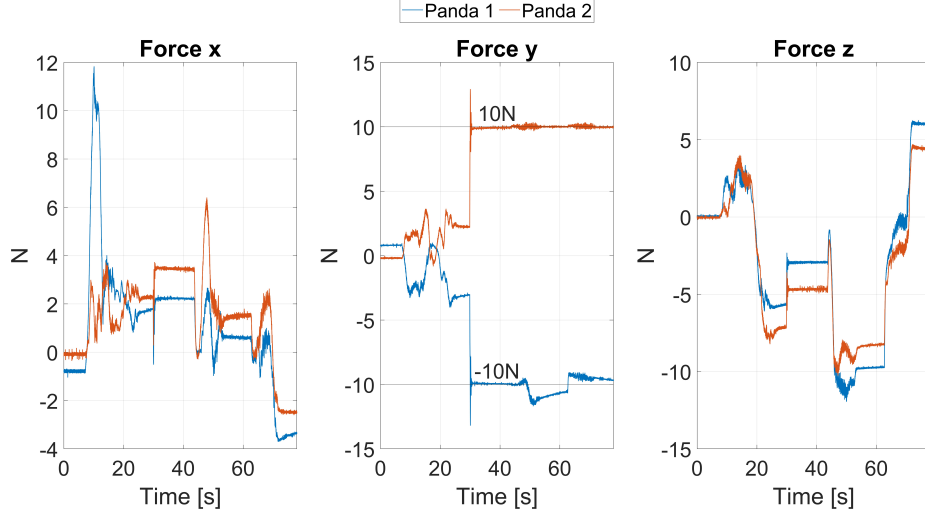


(d) object's pick-down

Fig. 7: Pick-up from random configuration task



(a) Pick-up task: Force controller results



(b) Pick-up task: Estimated Contact Force in global frame

A total of 18 pick-up tests were conducted under varying initial conditions. Out of these, 17 experiments yielded successful outcomes, achieving the task of picking up the box without any issues related to contact loss. In the one remaining experiment, the outcome was unsuccessful during the reaching phase. This failure was attributed to the initial condition of the end-effector, which was located at a singularity point of the human-like planner.

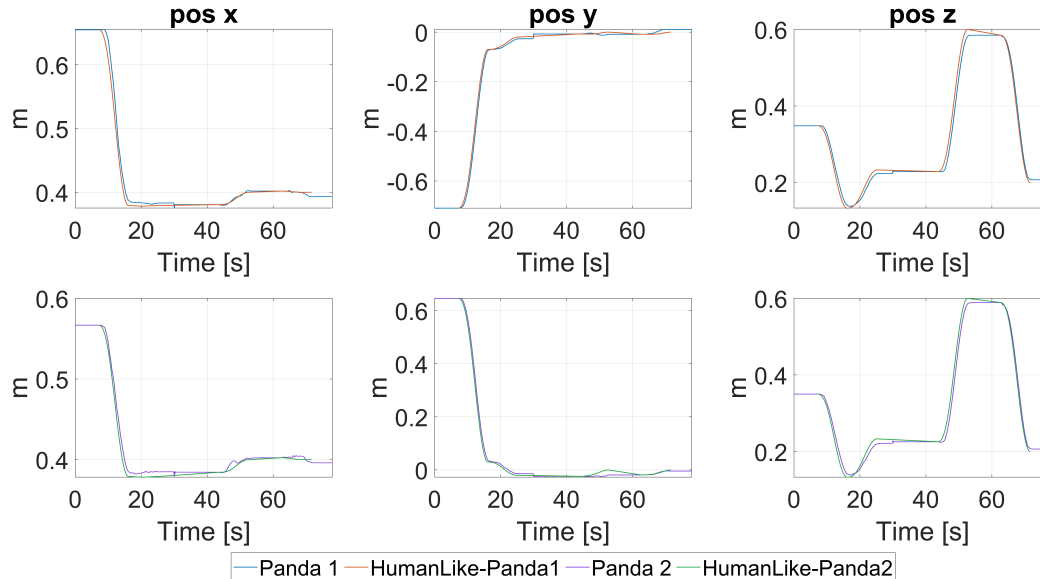
The output of the force control varies over time, as evident from the force graphs applied by the manipulators. This could be counterintuitive, as one might expect the end-effector has to exert a constant force to maintain a steady grasp on the object. To understand this behavior, we examine the contact forces graph, which show a deviation from the desired contact force value during the manipulation phase.

The force control system dynamically and efficiently adjusts the applied force of the end-effectors, aiming to converge the contact forces towards the desired value.

Therefore, it is likely that impedance control, through positional errors of the manipulators, indirectly causes these variations by attempting "compenetration" and "retraction." Force control quickly corrects these irregularities, ensuring grip stability and strength.

Despite vision imprecision and impedance control's positional errors, the hybrid control yields robust manipulation and grasping results. However, inadequate coupling can lead to unwanted rotations due to gravity, creating a moment around the grasp axis formed by the two end-effectors. There are two strategies to address this issue:

1. Increasing the contact force would guarantee that there is enough friction to offset the rotational moment.
2. Employing end-effectors that are softer or larger would increase the contact surface, enhance force exchange, and better compensate for misalignments brought on by the end-effectors' gravitational pull.



(c) Pick-up task: Human-Like desired Trajectory and Manipulators real trajectory

8.2 Payload mass estimation

Estimating forces at the end-effector tip allows the detection of both contact and weight forces. The weight force is transferred along the z-direction through contact friction. Accurate estimation is challenging due to the need for precise coordination between two robots. Position errors from Cartesian control and vision systems make perfect alignment of the end-effectors difficult, causing disturbance torques/forces that complicate force estimation. Additionally, end-effector rotation errors can distribute the weight force across multiple directions, hindering determination of the original weight force vector. Despite these challenges, precise weight force identification is possible if these specific conditions are minimized. According to specifications, the object's mass is 780 grams, resulting in a weight force of 7.6N.

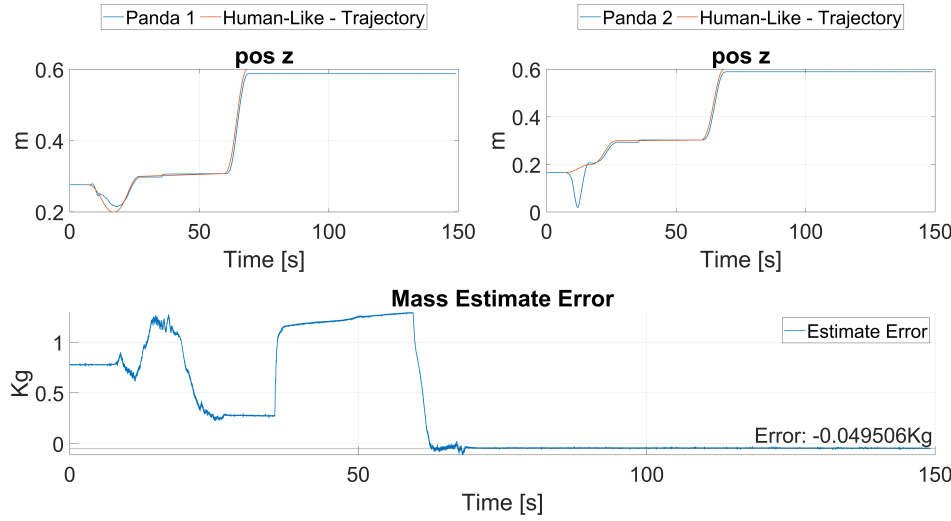


Fig. 8: Manipulators' Position along z-direction and Mass Estimate error result

The results obtained demonstrate that the estimation error stabilizes at 0.43 N at convergence. This is a remarkable result for the setup used, proving the usefulness of the chosen approach. The obtained accuracy is especially noteworthy in light of the starting conditions and variables, indicating that, provided the initial assumptions have been fulfilled, the applied model is reliable and well-suited to the particulars of the examined issue. This degree of accuracy guarantees consistency and dependability in the generated estimates and validates the viability of the selected method. It also opens the door for further applications in related scenarios.

9 Conclusion and Future Works

This thesis presents a hybrid control policy for dual object manipulations, addressing scenarios where other methods are insufficient.

The initial premises of achieving a stable and robust grasp were fully met, even with the introduction of the two preceding phases to manipulation. While these phases introduced some errors not present in case expressed in [4] where manipulators were already in a stable grasp, they did not compromise the object manipulation stage. Moreover, the introduction of reaching and the utilization of vision had no adverse impact on the outcomes of hybrid control.

Despite minor position and orientation errors, the manipulation was efficient and stable, as force control dynamically adjusted the end-effector's applied force to achieve desired contact forces. In conclusion the integration of vision and reaching was successful, though misalignments between end-effectors and contact points caused rotational moments due to gravity.

The thesis suggests future research directions, including integrating orientation into motion planning, improving payload mass estimation, enhancing impedance control, and expanding vision usage beyond initial scans for better accuracy. Utilizing post-grasp vision data could further improve manipulation precision, opening new avenues in robotics research.

Riferimenti bibliografici

- [1] M. Uchiyama and P. Dauchez, "Symmetric kinematic formulation and non-master/slave coordinated control of two-arm robots," *Advanced Robotics*, vol. 7, no. 4, pp. 361–383, 1992.
- [2] E. Nakano, "Cooperative control of the anthropomorphic manipulator melarm'." *Proc. of 4th Int. Symp. Industrial Robots.*, 1974.
- [3] F. Caccavale and M. Uchiyama, "Cooperative manipulation," *Springer handbook of robotics*, pp. 989–1006, 2016.
- [4] E. Shahriari, S. A. B. Birjandi, and S. Haddadin, "Passivity-based adaptive force-impedance control for modular multi-manual object manipulation," *IEEE Robotics and Automation Letters*, vol. 7, no. 2, pp. 2194–2201, 2022.
- [5] N. Dehio, J. Smith, D. L. Wigand, P. Mohammadi, M. Mistry, and J. J. Steil, "Enabling impedance-based physical human–multi–robot collaboration: Experiments with four torque-controlled manipulators," *The International Journal of Robotics Research*, vol. 41, no. 1, pp. 68–84, 2022.
- [6] K. Bouyarmane, K. Chappellet, J. Vaillant, and A. Kheddar, "Quadratic programming for multirobot and task-space force control," *IEEE Transactions on Robotics*, vol. 35, no. 1, pp. 64–77, 2018.
- [7] N. Hogan, "Impedance control of industrial robots," *Robotics and computer-integrated manufacturing*, vol. 1, no. 1, pp. 97–113, 1984.
- [8] A. De Luca, A. Albu-Schaffer, S. Haddadin, and G. Hirzinger, "Collision detection and safe reaction with the dlr-iii lightweight manipulator arm," in *2006 IEEE/RSJ International Conference on Intelligent Robots and Systems*. IEEE, 2006, pp. 1623–1630.
- [9] A. De Luca and R. Mattone, "Sensorless robot collision detection and hybrid force/motion control," in *Proceedings of the 2005 IEEE international conference on robotics and automation*. IEEE, 2005, pp. 999–1004.
- [10] S. Haddadin, "Evaluation criteria and control structures for safe human-robot interaction," Ph.D. dissertation, Technical University of Munich (TUM) & German Aerospace Center (DLR), 2005.
- [11] A. Nguyen and B. Le, "3d point cloud segmentation: A survey," in *2013 6th IEEE conference on robotics, automation and mechatronics (RAM)*. IEEE, 2013, pp. 225–230.
- [12] L. Ni and S. Jinhang, "The analysis and research of clustering algorithm based on pca," in *2017 13th IEEE International Conference on Electronic Measurement & Instruments (ICEMI)*. IEEE, 2017, pp. 361–365.
- [13] C. Bartneck, D. Kulic, E. Croft, and S. Zoghbi, "Measurement instruments for the anthropomorphism, animacy, likeability, perceived intelligence, and perceived safety of robots," *International journal of social robotics*, vol. 1, pp. 71–81, 2009.
- [14] L. D. Riek, T.-C. Rabinowitch, B. Chakrabarti, and P. Robinson, "How anthropomorphism affects empathy toward robots," in *Proceedings of the 4th ACM/IEEE international conference on Human robot interaction*, 2009, pp. 245–246.
- [15] M. Baracca, G. Averta, and M. Bianchi, "A general approach for generating artificial human-like motions from functional components of human upper limb movements," *Control Engineering Practice*, vol. 148, p. 105968, 2024.
- [16] M. Baracca, P. Bonifati, Y. Nisticò, V. Catrambone, G. Valenza, A. Bicchi, G. Averta, and M. Bianchi, "Functional analysis of upper-limb movements in the cartesian domain," in *Converging Clinical and Engineering Research on Neurorehabilitation IV: Proceedings of the 5th International Conference on Neurorehabilitation (ICNR2020), October 13–16, 2020*. Springer, 2022, pp. 339–343.
- [17] J. Ramsay and G. Hooker, "G., graves, s.,(2009). functional data analysis with r and matlab," *Springer-Verlag*, vol. 10, pp. 978–0.

- [18] G. Averta, F. Barontini, V. Catrambone, S. Haddadin, G. Handjaras, J. P. Held, T. Hu, E. Jakubowitz, C. M. Kanzler, J. Kühn *et al.*, “U-limb: A multi-modal, multi-center database on arm motion control in healthy and post-stroke conditions,” *GigaScience*, vol. 10, no. 6, p. giab043, 2021.
- [19] C. Ott, *Cartesian impedance control of redundant and flexible-joint robots*. Springer, 2008.